Article

Rigidification of Poly(*p*-phenylene)s through *ortho*-Phenyl Substitution

Anna Baun, Zuyuan Wang, Svenja Morsbach, Zijie Qiu, Akimitsu Narita, George Fytas, and Klaus Müllen*

Read Online

ACCESS | Metrics & More | Article Recommendations | Supporting Information

ABSTRACT: A sterically π-congested ortho-phenylated poly(*p*-phenylene) (PPP) has been synthesized with unprecedentedly high molecular weights up to 29 kDa after fractionation, as confirmed by gel permeation chromatography coupled with a multiangle laser light scattering detector. The chain translation diffusion coefficient obtained from dynamic light scattering experiments displayed strong scaling ($\sim L_w^{-0.8}$) to the chain contour length, indicating a rodlike shape with remarkably high rigidity of this novel PPP. These results provide an interesting insight into the relationship between the structure and the chain stiffness of PPP-based polymers and challenge the validity of the existing diffusion models in polymer physics.

- sterically π-congested *ortho*-phenylated PPP
- rod-like shape with remarkably high rigidity
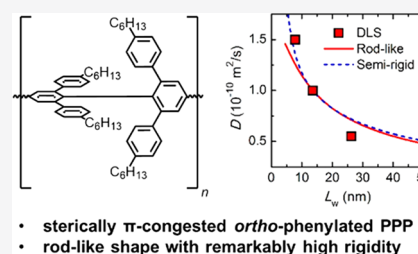
1. INTRODUCTION

The chain stiffness of polymers is characterized by the persistence length, which is a measure of the chain rigidity and allows for a clear distinction between flexible and rigid-rod polymers.[1] It can be understood as the distance over which the orientation of the bonds persists. Rigid-rod polymers with high stiffness, such as poly(*p*-phenylene terephthalamide) (PPTA, Kevlar)[2,3] and poly(*p*-phenylene benzobioxazole) (PBO)[4] with persistence lengths of ~20−50 nm, are used to prepare robust high-performance polymeric fibers, for a variety of applications including protective clothing and aerospace materials.[5,6] It is also important to have control over the persistence length of polymers to fine-tune their mechanical properties, but the relationship between the polymer structure and chain stiffness is still poorly understood.

Poly(*p*-phenylene)s (PPPs) represent a unique class of conjugated rigid-rod polymers.[7,8] Unsubstituted PPPs exhibit exceptional mechanical strength, stiffness, and high thermal stability due to the rigid aromatic backbone of the para-connected phenylene units.[9,10] Nevertheless, their applications are hampered by their vanishing solubility, which also induces structural defects and leads to low molecular weights during their preparations, typically through a Ni-mediated poly-condensation of aromatic dihalides[11] or an oxidative coupling of benzene in the presence of $CuCl_2$ and $AlCl_3$.[12,13] To circumvent these drawbacks, several protocols have been employed: (i) chemical transformation of solubilized precursor polymers to yield unsubstituted PPPs[14] and (ii) substitution of PPPs to enhance their solubility.[15−17] Especially, substituted PPPs bearing alkyl and/or additional functional groups have been studied as shape-persistent polymers. Notably, an additional concept used to prepare soluble PPPs with high molecular weights is to introduce regioirregularity through a suitable monomer choice or copolymerization, which unfortunately often lacks the structural perfection.[18−20]

The persistence lengths of representative PPP-based polymers are summarized in Table 1.[21−24] "Hairy rod" PPP **A** with aromatic sulfonate side chains showed a large persistence length of 25 nm. On the other hand, poly[9,9-bis(2-ethylhexyl)fluorine] **B**, with a partly planarized PPP backbone, exhibited a rather short persistence length (l_p = 7 nm). A similar persistence length (l_p = 8 nm) was observed for poly[6,6,12,12-tetrakis(2-ethylhexyl)-6,12-dihydrofluorene] **C**, despite its extended planarized segment, where rotation about interring bonds of the backbone was hindered.[22] In contrast, PPP-based polymer **D** with further extended planarized segments and bulkier alkylphenyl groups demonstrated a larger persistence length of 25 nm. On the other hand, PPP-based ladder polymer **E** displayed a rather short persistence length of 6.5 nm.[21] These results suggest that introduction of bulky substituents, rather than the "ladderization" of the backbone, drastically increases the persistence length. The prevailing structures would raise an intriguing question: given that the attachment of bulky substituents results in a significant rigidification of PPP-based polymers, as reported for **A** and **D** in comparison to **B**, **C**, and **E**, what is the stiffness of nonladder PPPs only bearing such substituents, causing significant interring rotations?
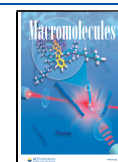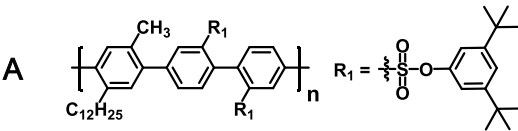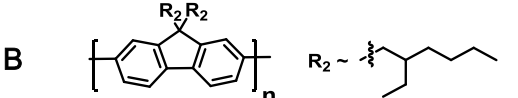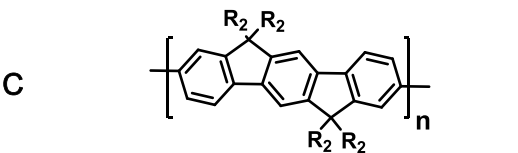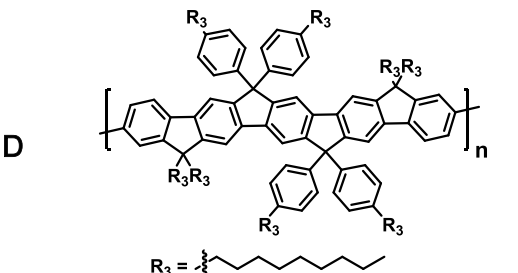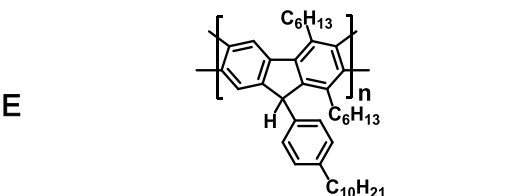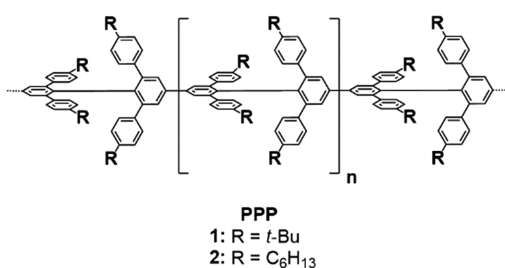
Table 1. Persistence Length (l_p) of Representative PPP-Based Polymers in the Literature

Polymer	Persistence length [nm]	Reference
A	25	21
B	7	22, 23
C	8	22
D	25	22
E	6.5	24

We have previously synthesized ortho-phenylated **PPP 1** consisting of sterically π-congested 2,2′,6,6′-tetraphenyl-1,1′-biphenyl units (Figure 1).[25] Every second interring bond of

**Figure 1.** Structure of ortho-phenylated PPPs **1** and **2**.

PPP 1 is surrounded by four *ortho*-phenyl substituents. While π-conjugation across these interring bonds is largely suppressed due to the pronounced torsion, **PPP 1** showed a remarkable bathochromic shift upon extension of the conjugation. This was attributed to a through-space conjugation among the π-orbitals of the phenyl substituents. A new intriguing question relates to the chain stiffness under the influence of this substitution. Nevertheless, the obtained ortho-phenylated PPPs were very short, with only up to 15 repeating

units, which hindered the investigation of their physical properties, in particular the persistence length.

In this work, we have achieved the synthesis of unprecedentedly long, ortho-phenylated **PPP 2** with weight-average molecular weight of up to 29 kDa, corresponding to a length of up to 35 repeating phenylene units within the backbone. By attaching hexyl chains at the para-positions of the phenyl substituents, the resulting polymers displayed high solubility in organic solvents (see below), in stark contrast to the previous **PPP 1** with *tert*-butyl groups, which displayed scarce solubility. By performing dynamic light scattering studies, we could disclose a remarkably high rigidity of **PPP 2** with the persistence length exceeding the highest examined contour length.

2. RESULTS AND DISCUSSION

In our previous work, the short length of the obtained *tert*-butyl functionalized **PPP 1** could be attributed to a low reactivity of the dichloro-functionalized monomers during the Ni^0-mediated Yamamoto polycondensation.[26] Moreover, we observed precipitation of the oligomers during the polymerization, which indicated that the *tert*-butyl groups did not provide sufficient solubility. To achieve higher molecular weights, we designed 2,2′,6,6′-tetrakis(hexylphenyl)-4,4′-bistri-

Scheme 1. Synthetic Route toward Monomer 6 and Its Polymerization to PPP 2[a]
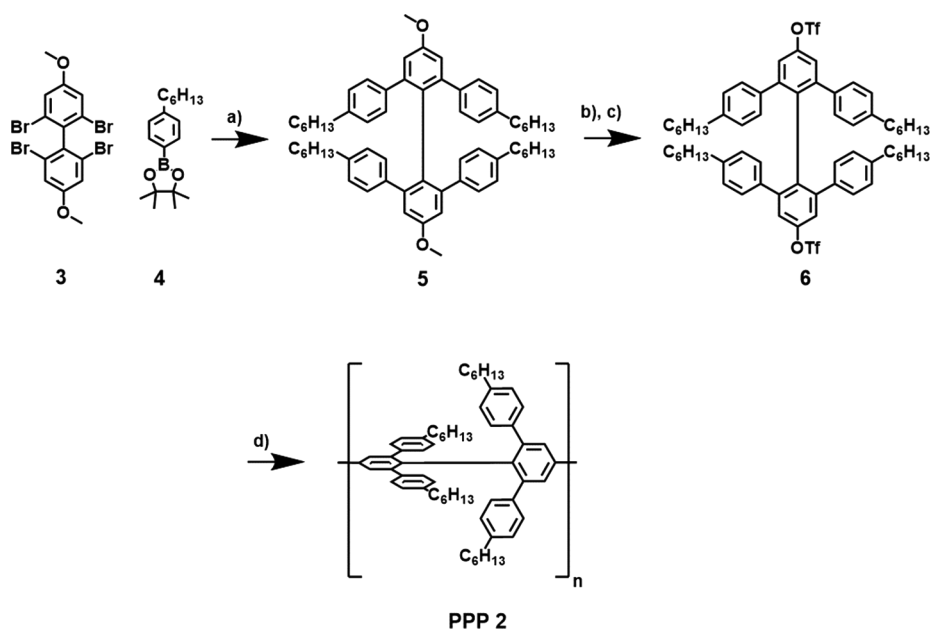
flate-1,1′-biphenyl (6) as the monomer (Scheme 1). Triflate groups were chosen instead of the chloro groups, considering their higher reactivity for the Yamamoto coupling reaction and relative ease of introduction, compared with bromo or iodo groups.[27−29] Hexyl groups were chosen as the solubilizing substituents to ensure higher solubility of the resulting polymers. The synthesis of monomer 6 bearing triflates at the 4,4′-positions was carried out through a 4-fold Suzuki-Miyaura coupling as displayed in Scheme 1.

On the basis of literature procedures,[30,31] 2,2′,6,6′-tetrabromo-4,4′-dimethoxy-1,1′-biphenyl (3) was prepared by a three-step synthesis through diazotation of 2,4,6-tribromoaniline followed by an oxidative dimerization using CuCl₂ and then selective aromatic nucleophilic substitution of only the two bromo atoms at the 4,4′-positions in the presence of sodium methoxide (Supporting Information). Subsequent Suzuki-Miyaura coupling of 3 with boronate ester 4 led to 2,2′,6,6′-tetrakis(hexylphenyl)-4,4′-dimethoxy-1,1′-biphenyl (5) in 43% yield. The methoxy groups of 5 were converted to hydroxy groups by treatment with boron tribromide, and the resulting bisphenol was directly reacted with trifluoromethanesulfonic acid anhydride (Tf₂O) and pyridine in dichloromethane to provide bistriflate monomer 6 in 90% yield over two steps. The structure of 6 was confirmed by ¹H and ¹³C NMR spectroscopy and matrix-assisted laser desorption/ionization time-of-flight (MALDI-TOF) mass spectrometry (MS) (Figure S4−S6).

The polymerization of monomer 6 was performed through the Yamamoto polycondensation. The reaction proceeded at a relatively high monomer concentration (50 mM) without obvious formation of cyclic oligomers according to size-exclusion chromatography (SEC) analysis. First, the synthesis of PPP 2 was carried out via the procedure previously described for PPP 1, using a catalyst system consisting of bis(1,5-cyclooctadiene)nickel(0) [Ni(COD)₂], 2,2′-bipyridyl, and 1,5-cyclooctadiene (COD) in a toluene/dimethylformamide mixture by microwave-assisted heating at 90 °C for 24 h.

Nevertheless, only oligomers with low weight-average molecular weight (M_w) up to 5 kDa could be obtained, based on SEC analysis (tetrahydrofuran (THF), PPP standard) (Table S1). When using THF as a solvent, PPP 2 with higher M_w of 18.9 kDa was formed in 89% yield after 3 h. A relatively broad distribution indicated by the polydispersity (PDI) of 1.9 based on the SEC analysis is in the expected range for a step-growth polymerization. PPP 2 exhibited good solubility in common organic solvents such as THF, chloroform, and toluene. MALDI-TOF MS characterization displayed the presence of a regular pattern with peak-to-peak distances corresponding to the mass of a monomer unit, only with signals assignable to PPP 2 (Figure 2a). Molecular weights up to 40−50 kDa were observed, corresponding to a length of ∼60 repeating units. The UV/vis absorption spectra demonstrated a bathochromic shift of the absorption maximum upon the polymerization, from 265 nm (monomer 6) to 340 nm (PPP 2) (Figures 2c). Further, PPP 2 showed a broad blue emission from 380 nm up to 420 nm, in agreement with the previously described PPP 1. In this regard, the through-space conjugation via the phenyl substituents seems to maintain extended conjugation along the PPP backbone in spite of the unfavorable interring torsion.

Preparative recycling SEC allowed for the separation of PPP 2 into monodisperse fractions PPP 2−1, PPP 2−2, and PPP 2−3 (see Table S1 and Figure S9−11 for details). The absolute M_w was obtained by gel permeation chromatography coupled with a multiangle laser light scattering detector (GPC-MALLS). The light scattering intensity was found to be independent of the scattering angle (θ) for all three fractions suggesting a small radius of gyration, R_g (<20 nm). The values of absolute M_w were calculated from the light scattering intensity using the experimental refractive index increment, $dn/dc = (0.286 \pm 0.002)$ cm³/g in THF at 293 K to be $M_w =$ 29.4 kDa (PPP 2−1, PDI = 1.1), 15.3 kDa (PPP 2−2, PDI = 1.1), and 8.8 kDa (PPP 2−3, PDI = 1.1) (Table S1).

In order to assess the stiffness of PPP 2, we would ideally need the form factor and the two transport (translation and
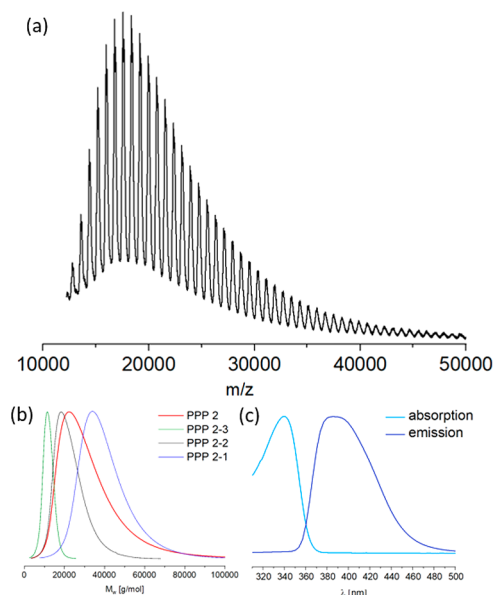
Figure 2. (a) Linear-mode MALDI-TOF MS spectra of **PPP 2**; matrix: *trans*-2-[3-(4-*tert*-butylphenyl)-2-methyl-2-propenylidene]-malononitrile (DCTB). (b) Molecular-weight distributions of **PPP 2** and polymeric fractions **PPP 2−1**, **PPP 2−2**, and **PPP 2−3** (SEC, THF, and PPP standard). (c) Normalized UV/vis absorption and emission spectra of **PPP 2** (10^{-6} M in dichloromethane).

Figure 3. Relaxation functions $C(q, t)$ for the translational motion of two fractions of **PPP 2** with long (**PPP 2−1**, black ○) and short (**PPP 2−3**, red ○) molecular weight fractions in THF at a scattering wave vector $q = 0.0197$ nm^{-1} and at 293 K. The solid lines denote the representation of the $C(q, t)$ by a double exponential decay fit. The translational diffusion coefficients D of **PPP 2−1** and **PPP 2−3** chains and the associated scattering intensities obtained from the fast decay of $C(q, t)$ are shown in the upper and lower insets, respectively, using the same colors for two **PPP 2** fractions. The horizontal solid lines in the two insets denote the average values of the depicted quantities.

rotation) coefficients of at least two polymer fractions. The former can be recorded by neutron scattering (NS) and/or static light scattering (SLS) depending on the polymer size, whereas the latter are accessible by dynamic light scattering (DLS). In the present case, the form factor (and hence R_g) cannot be obtained by SLS due to the small size and the low light scattering wave vector, q, i.e., $qR_g \ll 1$. However, utilization of NS or X-ray scattering techniques[32−34] with high spatial resolution requires higher concentrations than SLS, which is often a disadvantage due to aggregation. Therefore, the three polymer fractions, **PPP 2−1**, **PPP 2−2**, and **PPP 2−3** were investigated by DLS.[1,25] Figure 3 shows the relaxation function, $C(q, t)$, for dilute solutions of **PPP 2−1** (black symbols) and **PPP 2−3** (red symbols) in THF at 293 K. The magnitude of the scattering wave vector q depends on the scattering angle θ as $q = (4\pi n/\lambda)\sin(\theta/2)$, where n is the refractive index of the solvent THF and $\lambda = 632$ nm is the laser wavelength. The value of q controls the length, $2\pi/q$, over which the chain diffusion is probed. For example, $q = 0.0197$ nm^{-1} (in Figure 3) corresponds to a diffusion length of about 320 nm. For both fractions, $C(q, t)$ is not unimodal as would be expected in the case of single scattering moieties in dilute solutions. Instead, a bimodal shape due to the presence of a fast and slow relaxation process is resolved through a double exponential representation of the $C(q, t)$ (solid black and red lines in Figure 3). The resolved dynamics are both diffusive as the two characteristic relaxation rates, $\Gamma(q)$, are q^2 dependent allowing the calculation of the two, slow and fast, translational diffusion coefficients, $D = \Gamma(q)/q^2$. Hence, the two processes are assigned to two species: **PPP 2** aggregates with slow D_s and single **PPP 2** chains, with fast D. This assignment is verified by the q-independent intensity of the fast process in both fractions, as shown in the lower inset of Figure 3. According to this finding, the magnification, $qR_g \ll 1$, is low due to the small radius of gyration, R_g. Consistently, the fast diffusion

coefficient, $D = \Gamma(q)/q^2$ of the **PPP 2**, is virtually q-independent (upper inset to Figure 3) due to the absence of internal dynamics contribution at high q's.[1]

The presence of aggregates even at very low concentrations renders the use of DLS and not SLS necessary for a correct determination of M_w. The M_w values of the three **PPP 2** fractions estimated from the intensity of the fast process are in good agreement with the M_w obtained from the GPC-MALLS at sufficiently low concentrations. As already mentioned, for the short **PPP 2−3**, $qR_g \ll 1$, and therefore the radius of gyration is not accessible with the low q's in SLS experiments. This problem can be resolved by using **PPP 2** with a higher M_w and hence a larger R_g or by conducting neutron or X-ray experiments which allow accessing much higher q's.[32−34] The latter, however, would require much higher **PPP 2** concentrations, hampered by aggregation issues. Hence for short chains, information on the polymer conformation can only be extracted from the chain translational diffusion coefficient. Access to the rotational chain diffusion coefficient[1] is usually not feasible due to extremely low depolarized light scattering in very dilute solutions without an additional resonance-based enhancement.[35]

The availability of three different polymer fractions with known weight-average molecular weight (M_w) allows one to access the chain conformation on the premise of M_w, independent persistence length (l_p), and the validity of the diffusion models for thin backbone polymer chains. The values of M_w and the contour length $L_w = (M_w/M_n)l_m$, with $M_n = 795.3$ g/mol and $l_m = 0.7$ nm being the monomer molecular weight and length, respectively, are listed in Table 2. The hydrodynamic radius R_h is computed from the experimental D as $R_h = k_B T/(6\pi\eta D)$, where k_B, T, and η are the Boltzmann constant, absolute temperature, and shear viscosity of the solvent, respectively. The R_h values are listed in Table 2 as diameters, $d_h = 2R_h$. The ratio d_h/L_w provides the first evidence of an approximately rigid chain conformation, as the factor (2.74) of increase in the hydrodynamic diameter from **PPP 2−**

Table 2. Molecular Characteristics and Physical Properties

	M_w [kg/mol] ($\pm 2\%$)	L_w [nm]	D [10^{-10} m^2/s] ($\pm 2\%$)	$2R_h$ [nm]	d_h/L_w
PPP2−3	8.8	7.8	1.50	5.8	0.74
PPP2−2	15.3	13.6	1.00	8.8	0.65
PPP2−1	29.5	26.2	0.55	15.9	0.61

3 to **PPP 2−1** is closer to the factor of 3.35 expected for rigid-rod chains ($d_H \sim L_w^1$) than to the factor of 1.8 expected for random-coil chains ($d_H \sim L_w^{1/2}$). However, the systematic decrease of d_h/L_w with L_w suggests a weaker than L_w^1 dependence as discussed next.

Figure 4a provides a plot of the translational diffusion coefficient D versus the chain length L_w for the three fractions
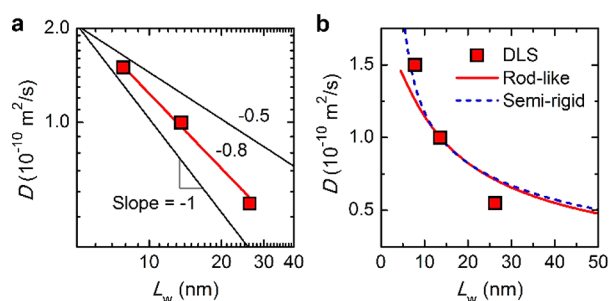
Figure 4. Translational diffusion coefficient D vs contour length L_w in a log−log (a) and linear (b) representation for the three fractions of **PPP 2**. The black lines in panel (a) have slopes of −1 and −0.5, corresponding to the scaling relations for rigid-rod and Gaussian-coil chains, respectively. The red line in panel (b) is based on a rodlike-chain model [eq (S3)] with $L_{RR} = L_w$ and $d_{RR} = 4.7$ nm. The blue dashed line in panel (b) based on a semirigid-chain model [eq (S1)] with $L_K = L_w$ and $d_H = 3.0$ nm. The experimental error ($\pm 2\%$) is smaller than the size of the symbols.

of **PPP 2**. Assuming a scaling behavior $D \sim L_w^{-\nu}$, well established for thin flexible polymer chains, the double-logarithmic presentation in Figure 4a yields the scaling exponent ν; $\nu = 0.5$ for theta and $\nu \approx 0.6$ for good solvent conditions. Unexpectedly, **PPP 2** displays a strong decrease of D with molecular weight represented by an effective exponent $\nu = 0.8$. This implies a much more extended chain conformation than for a Gaussian coil with the same number of monomers. Quantitatively, for the highest M_w fraction, D is 270% slower than for the same chain with an ideal (Gaussian) conformation. Thus, the model-independent plot of Figure 4a clearly suggests an extreme persistency of the **PPP 2** chains.

In order to estimate the persistence length, l_p, the experimental $D(L_w)$ needs to be represented by the known models of chain diffusion in dilute solutions. These are the semirigid[36] or rodlike model,[37] which are derived for chains with rather thin monomer units.[38−40] We also note that the theoretical representation of $D(L_w)$ without additional information, e.g., rotational diffusion or R_g, requires an estimation of the chain diameter.

For a semirigid chain with a Kuhn segment,[41] $l_K = 2l_p$, the translational diffusion coefficient depends on L_w, l_K, and the chain "hydrodynamic" diameter d_H. Due to its dynamic nature, the value of d_H might deviate from its monomer counterpart. The semirigid model [eq (S1)] captures the rigid and coil-chain conformations in the limits $l_w/l_K < 1$ and $l_w/l_K \gg 1$, respectively. The experimental $D(L_w)$ of the three **PPP 2**

fractions can be represented (dashed line in Figure 4b) by $l_w/l_K = 1$ (rigid-rod limit), but the value of d_H increases from 2.4 nm (**PPP 2−3**) to 5.1 nm (**PPP 2−1**) (Figure S12). We note that the $D(L_w)$ slope appears steeper in the semirigid than in the rigid-rod representation (dashed blue line vs solid red line in Figure 4b). This counterintuitive observation is due to the different mathematical expressions of the semirigid chain model in the rigid-rod limit and the rodlike chain model. Therefore, the two models have inherently different dependence on d_H and d_{RR} (Figure S13). While the chain conformation corresponds to a rigid rod, the increase of d_H with L_w might imply variation of the hydrodynamic flow with L_w. On the basis of molecular mechanics calculations for **PPP 2** trimer, the monomer diameter was estimated to be ~2 nm by analyzing the conformation of the middle repeating unit in the trimer (Figure S14). The simulated value is smaller than the hydrodynamic d_H, which is expected considering that the assumed stick boundary diffusion conditions imply solvation of **PPP 2**. In addition, the experimental D represents an average translational diffusion parallel and normal to the long axis of the rodlike chain. For semirigid bottle-brush polymers,[42,43] and dendronized polymers[34] cross-sectional radii between 2 and 4 nm have been reported.

The value of d_H depends on the molecular weight distribution, M_w/M_n, which impacts the polymer translation diffusion. For semirigid chains, the effect of the size polydispersity on D has been theoretically considered assuming a Schulz-Zimm size polydispersity distribution.[44] For Schulz-Zimm-like size polydispersity with $M_w/M_n = 1.1$ (Table S1), the computed D [eq (S2)] is about 6% lower than that for $M_w/M_n = 1$. To represent the experimental D, the value of diameter d_H is thinner by 11% compared to the value for $M_w/M_n = 1$.

Since the diffusion model for semirigid chains represents the present data, but in the rigid-rod limit of its applicability, it is reasonable to examine the experimental $D(L_w)$ using a model for rodlike chains [eq (S3)].[37] Here, D depends on both the length L_{RR} and diameter d_{RR} of the rigid rod, which are used as adjustable parameters. While L_{RR} should be somewhat lower, but proportional to the chain contour length L_w, the effective monomer d_{RR} should not depend on L_w. The predicted D of a thick rod using a constant $d_{RR} = 4.7$ nm and $L_{RR} = L_w$ deviates from the experimental D's for the low and high M_w fractions of **PPP 2**, as indicated by the solid line in Figure 4b. In fact, this disparity is due to the monotonic increase of d_{RR} from 2.4 nm (**PPP 2−3**) to 5.1 nm (**PPP 2−1**) (Figure S12). Since a similar trend was revealed for the diameter d_H of the semirigid chain model and noting the similar quality of the two fits (solid and dashed lines in Figure 4b), the validity of these models for thick chains is questionable. This has been also argued in the case of dendronized polymers.[34] Therefore, the advanced chemistry of polymers with thick monomer structures[33,34,42,43,45] challenges the existing polymer diffusion models.

3. CONCLUSION

In conclusion, we have subjected sterically π-congested 2,2′,6,6′-tetraphenyl-1,1′-biphenyl **6**, bifunctionalized in its 4,4′-positions to Yamamoto polycondensation yielding unprecedentedly long and soluble ortho-phenylated **PPP 2**. Preparative recycling SEC furnished polymeric fractions, which were then analyzed by SEC and GPC-MALLS. To estimate the chain persistency, the translational diffusion coefficients, Ds, for three fractions of **PPP-2** were determined by dynamic light

scattering. The rodlike shape of the **PPP-2** chains was unambiguously established by the strong dependence of D on the chain contour length, L_w. The persistence length is expected to exceed the highest examined contour length (~25 nm). Further, the observed semiquantitative comparison with the two main polymer diffusion models can stimulate new theoretical studies of ultrarigid polymers, which will yield new insights into the design of PPP polymers for applications where shape is important.

■ ASSOCIATED CONTENT

⒮ Supporting Information

The Supporting Information is available free of charge at https://pubs.acs.org/doi/10.1021/acs.macromol.0c00810.

> Experimental details, NMR and MALDI-TOF MS spectra of all synthesized compounds, semirigid chain model calculations and computational details (PDF)

■ AUTHOR INFORMATION

Corresponding Author

Klaus Müllen − *Max Planck Institute for Polymer Research, 55128 Mainz, Germany;* ⓞ orcid.org/0000-0001-6630-8786; Email: muellen@mpip-mainz.mpg.de

Authors

Anna Baun − *Max Planck Institute for Polymer Research, 55128 Mainz, Germany*

Zuyuan Wang − *Max Planck Institute for Polymer Research, 55128 Mainz, Germany;* ⓞ orcid.org/0000-0002-3174-4227

Svenja Morsbach − *Max Planck Institute for Polymer Research, 55128 Mainz, Germany;* ⓞ orcid.org/0000-0001-9662-8190

Zijie Qiu − *Max Planck Institute for Polymer Research, 55128 Mainz, Germany;* ⓞ orcid.org/0000-0003-0728-1178

Akimitsu Narita − *Max Planck Institute for Polymer Research, 55128 Mainz, Germany;* ⓞ orcid.org/0000-0002-3625-522X

George Fytas − *Max Planck Institute for Polymer Research, 55128 Mainz, Germany; FORTH, Institute of Electronic Structure and Laser, 70013 Heraklion, Crete, Greece*

Complete contact information is available at:
https://pubs.acs.org/10.1021/acs.macromol.0c00810

Author Contributions

The manuscript was written through contributions of all authors. All authors have given approval to the final version of the manuscript.

Notes

The authors declare no competing financial interest.

■ ACKNOWLEDGMENTS

■ REFERENCES

(1) Wunderlich, K.; Müllen, K.; Fytas, G. Shape Persistence in Polymers and Supramolecular Assemblies. *Mater. Energy* **2018**, 1−28.

(2) Arpin, M.; Strazielle, C. Characterization and conformation of aromatic polyamides: poly(1,4-phenylene terephthalamide) and poly(p-benzamide) in sulphuric acid. *Polymer* **1977**, *18*, 591−598.

(3) Cotts, P. M.; Berry, G. C. Studies on dilute solutions of rodlike macroions. II. Electrostatic effects. *J. Polym. Sci., Polym. Phys. Ed.* **1983**, *21*, 1255−1274.

(4) Wong, C.-P.; Ohnuma, H.; Berry, G. C. Properties of some rodlike polymers in solution. *J. Polym. Sci., Polym. Symp.* **1978**, *65*, 173−192.

(5) Afshari, M.; Sikkema, D. J.; Lee, K.; Bogle, M. High Performance Fibers Based on Rigid and Flexible Polymers. *Polym. Rev.* **2008**, *48*, 230−274.

(6) Hu, X.-D.; Jenkins, S. E.; Min, B. G.; Polk, M. B.; Kumar, S. Rigid-Rod Polymers: Synthesis, Processing, Simulation, Structure, and Properties. *Macromol. Mater. Eng.* **2003**, *288*, 823−843.

(7) Wang, D. H.; Jiang, H.; Wade Adams, W. Rigid-Rod Polymers. *Encyclopedia of Polymer Science and Technology*; John Wiley & Sons, Inc., 2011, DOI: 10.1002/0471440264.pst323.pub2.

(8) Qiu, Z.; Hammer, B. A. G.; Müllen, K. Conjugated polymers − Problems and promises. *Prog. Polym. Sci.* **2020**, *100*, 101179.

(9) Marvel, C. S.; Hartzell, G. E. Preparation and Aromatization of Poly-1,3-cyclohexadiene1. *J. Am. Chem. Soc.* **1959**, *81*, 448−452.

(10) Friedrich, K.; Burkhart, T.; Almajid, A. A.; Haupert, F. Poly-Para-Phenylene-Copolymer (PPP): A High-Strength Polymer with Interesting Mechanical and Tribological Properties. *Int. J. Polym. Mater.* **2010**, *59*, 680−692.

(11) Yamamoto, T.; Hayashi, Y.; Yamamoto, A. A Novel Type of Polycondensation Utilizing Transition Metal-Catalyzed C−C Coupling. I. Preparation of Thermostable Polyphenylene Type Polymers. *Bull. Chem. Soc. Jpn.* **1978**, *51*, 2091−2097.

(12) Kovacic, P.; Oziomek, J. p-Polyphenyl from Benzene—Lewis Acid Catalyst—Oxidant. Reaction Scope and Investigation of the Benzene—Aluminum Chloride—Cupric Chloride System1. *J. Org. Chem.* **1964**, *29*, 100−104.

(13) Toshima, N.; Kanaka, K.; Koshirai, A.; Hirai, H. The Polymerization of Benzene Catalyzed by a Copper(I) Chloride−Aluminium Chloride−Oxygen System. *Bull. Chem. Soc. Jpn.* **1988**, *61*, 2551−2557.

(14) Abdulkarim, A.; Hinkel, F.; Jänsch, D.; Freudenberg, J.; Golling, F. E.; Müllen, K. A New Solution to an Old Problem: Synthesis of Unsubstituted Poly(para-phenylene). *J. Am. Chem. Soc.* **2016**, *138*, 16208−16211.

(15) Rehahn, M.; Schlüter, A.-D.; Wegner, G.; Feast, W. J. Soluble poly(para-phenylene)s. 1. Extension of the Yamamoto synthesis to dibromobenzenes substituted with flexible side chains. *Polymer* **1989**, *30*, 1054−1059.

(16) Rehahn, M.; Schlüter, A.-D.; Wegner, G.; Feast, W. J. Soluble poly(para-phenylene)s. 2. Improved synthesis of poly(para-2,5-di-n-hexylphenylene) via Pd-catalysed coupling of 4-bromo-2,5-di-n-hexylbenzeneboronic acid. *Polymer* **1989**, *30*, 1060−1062.

(17) Rehahn, M.; Schlüter, A.-D.; Wegner, G. Soluble poly(para-phenylene)s, 3. Variation of the length and the density of the solubilizing side chains. *Makromol. Chem.* **1990**, *191*, 1991−2003.

(18) Grob, M. C.; Feiring, A. E.; Auman, B. C.; Percec, V.; Zhao, M.; Hill, D. H. Solubilization of Regioregular and Regioirregular Poly(p-phenylene)s via CF3 and OCF3 Substituents To Generate a Model for Rigid-Rod Polymers. *Macromolecules* **1996**, *29*, 7284−7293.

(19) Percec, V.; Zhao, M.; Bae, J.-Y.; Hill, D. H. Regioregular and Regioirregular Poly(p-phenylene)s via Ni(0)-Catalyzed Homocoupling of Arylene Bismesylates. *Macromolecules* **1996**, *29*, 3727−3735.

(20) Percec, V.; Asandei, A. D.; Hill, D. H.; Crawford, D. Poly(p-phenylene)s with Mesogenic Side Groups: A Potential Class of NII Side Chain Liquid Crystalline Polymers? *Macromolecules* **1999**, *32*, 2597−2604.

(21) Petekidis, G.; Vlassopoulos, D.; Fytas, G.; Rülkens, R.; Wegner, G. Orientation Dynamics and Correlations in Hairy-Rod Polymers: Concentrated Regime. *Macromolecules* **1998**, *31*, 6129−6138.

(22) Somma, E.; Loppinet, B.; Fytas, G.; et al. Collective orientation dynamics in semi-rigid polymers. *Colloid Polym. Sci.* **2004**, *282*, 867−873.

(23) Grell, M.; Bradley, D. D. C.; Long, X.; Chamberlain, T.; Inbasekaran, M.; Woo, E. P.; Soliman, M. Chain geometry, solution

aggregation and enhanced dichroism in the liquidcrystalline conjugated polymer poly(9,9-dioctylfluorene). *Acta Polym.* **1998**, *49*, 439−444.

(24) Petekidis, G.; Fytas, G.; Scherf, U.; Müllen, K.; Fleischer, G. Dynamics of poly(p-phenylene) ladder polymers in solution. *J. Polym. Sci., Part B: Polym. Phys.* **1999**, *37*, 2211−2220.

(25) Schlütter, F.; Nishiuchi, T.; Enkelmann, V.; Müllen, K. π-Congested poly(paraphenylene) from 2,2′,6,6′-tetraphenyl-1,1′-biphenyl units: synthesis and structural characterization. *Polym. Chem.* **2013**, *4*, 2963−2967.

(26) Schlüter, F.; Nishiuchi, T.; Enkelmann, V.; Müllen, K. π-Congested poly(paraphenylene) from 2,2′,6,6′-tetraphenyl-1,1′-biphenyl units: synthesis and structural characterization. *Polym. Chem.* **2013**, *4*, 2963−2967.

(27) Beinhoff, M.; Bozano, L. D.; Scott, J. C.; Carter, K. R. Design and Synthesis of New Polymeric Materials for Organic Nonvolatile Electrical Bistable Storage Devices: Poly(biphenylmethylene)s. *Macromolecules* **2005**, *38*, 4147−4156.

(28) Percec, V.; Bae, J.-Y.; Zhao, M.; Hill, D. H. Aryl Mesylates in Metal-Catalyzed Homocoupling and Cross-Coupling Reactions. 1. Functional Symmetrical Biaryls from Phenols via Nickel-Catalyzed Homocoupling of Their Mesylates. *J. Org. Chem.* **1995**, *60*, 176−185.

(29) Rosen, B. M.; Quasdorf, K. W.; Wilson, D. A.; Zhang, N.; Resmerita, A.-M.; Garg, N. K.; Percec, V. Nickel-Catalyzed Cross-Couplings Involving Carbon-Oxygen Bonds. *Chem. Rev.* **2011**, *111*, 1346−1416.

(30) Trusova, M. E.; Krasnokutskaya, E. A.; Postnikov, P. S.; Choi, Y.; Chi, K.-W.; Filimonov, V. D. A Green Procedure for the Diazotization-Iodination of Aromatic Amines under Aqueous, Strong-Acid-Free Conditions. *Synthesis* **2011**, *2011*, 2154−2158.

(31) Graff, J.; Debande, T.; Praz, J.; Guénée, L.; Alexakis, A. Asymmetric Bromine−Lithium Exchange: Application toward the Synthesis of Natural Product. *Org. Lett.* **2013**, *15*, 4270−4273.

(32) Fytas, G.; Nothofer, H. G.; Scherf, U.; Vlassopoulos, D.; Meier, G. Structure and Dynamics of Nondilute Polyfluorene Solutions. *Macromolecules* **2002**, *35*, 481−488.

(33) Förster, S.; Neubert, I.; Schlüter, A. D.; Lindner, P. How Dendrons Stiffen Polymer Chains: A SANS Study. *Macromolecules* **1999**, *32*, 4043−4049.

(34) Dutertre, F.; Bang, K.-T.; Vereroudakis, E.; Loppinet, B.; Yang, S.; Kang, S.-Y.; Fytas, G.; Choi, T.-L. Conformation of Tunable Nanocylinders: Up to Sixth-Generation Dendronized Polymers via Graft-Through Approach by ROMP. *Macromolecules* **2019**, *52*, 3342−3350.

(35) Koch, A. H. R.; Lévêque, G.; Harms, S.; Jaskiewicz, K.; Bernhardt, M.; Henkel, A.; Sönnichsen, C.; Landfester, K.; Fytas, G. Surface Asymmetry of Coated Spherical Nanoparticles. *Nano Lett.* **2014**, *14*, 4138−4144.

(36) Ortega, A.; Garcıa de la Torre, J. Hydrodynamic properties of rodlike and disklike particles in dilute solution. *J. Chem. Phys.* **2003**, *119*, 9914−9919.

(37) Forero-Martinez, N. C.; Baumeier, B.; Kremer, K. Backbone Chemical Composition and Monomer Sequence Effects on Phenylene Polymer Persistence Lengths. *Macromolecules* **2019**, *52*, 5307−5316.

(38) Hsu, H.-P.; Paul, W.; Rathgeber, S.; Binder, K. Characteristic Length Scales and Radial Monomer Density Profiles of Molecular Bottle-Brushes: Simulation and Experiment. *Macromolecules* **2010**, *43*, 1592−1601.

(39) Binder, K.; Hsu, H.-P.; Paul, W. Understanding the stiffness of macromolecules: From linear chains to bottle-brushes. *Eur. Phys. J.: Spec. Top.* **2016**, *225*, 1663−1671.

(40) Milchev, A.; Binder, K. Linear Dimensions of Adsorbed Semiflexible Polymers: What Can Be Learned about Their Persistence Length? *Phys. Rev. Lett.* **2019**, *123*, 128003.

(41) Harnau, L.; Winkler, R. G.; Reineker, P. Dynamic properties of molecular chains with variable stiffness. *J. Chem. Phys.* **1995**, *102*, 7750−7757.

(42) Zhang, B.; Grohn, F.; Pedersen, J. S.; Fischer, K.; Schmidt, M. Conformation of Cylindrical Brushes in Solution: Effect of Side Chain Length. *Macromolecules* **2006**, *39*, 8440−8450.

(43) Rathgeber, S.; Pakula, T.; Wilk, A.; Matyjaszewski, K.; Lee, H.-i.; Beers, K. L. Bottle-brush macromolecules in solution: Comparison between results obtained from scattering experiments and computer simulations. *Polymer* **2006**, *47*, 7318−7327.

(44) Harnau, L.; Winkler, R. G.; Reineker, P. Influence of Polydispersity on the Dynamic Structure Factor of Macromolecules in Dilute Solution. *Macromolecules* **1999**, *32*, 5956−5960.

(45) Bates, C. M.; Chang, A. B.; Momčilović, N.; Jones, S. C.; Grubbs, R. H. ABA Triblock Brush Polymers: Synthesis, Self-Assembly, Conductivity, and Rheological Properties. *Macromolecules* **2015**, *48*, 4967−4973.